Atmos. Chem. Phys. Discuss., 9, 8587–8618, 2009
www.atmos-chem-phys-discuss.net/9/8587/2009/
© Author(s) 2009. This work is distributed under
the Creative Commons Attribution 3.0 License.

Atmospheric Chemistry and Physics Discussions

This discussion paper is/has been under review for the journal *Atmospheric Chemistry and Physics (ACP)*. Please refer to the corresponding final paper in *ACP* if available.

The impact of resolution on ship plume simulations with NO_x chemistry

C. L. Charlton-Perez[1,2], M. J. Evans[1], J. H. Marsham[1], and J. G. Esler[2]

[1]Institute for Atmospheric Science, The School of the Environment, University of Leeds, Leeds, UK
[2]Department of Mathematics, University College London, London, UK

Received: 25 January 2009 – Accepted: 26 January 2009 – Published: 31 March 2009

Correspondence to: C. L. Charlton-Perez (cristina.l.perez@gmail.com)

Published by Copernicus Publications on behalf of the European Geosciences Union.

Abstract

A high resolution chemical transport model of the marine boundary layer is designed in order to investigate the detailed chemical evolution of a ship plume. To estimate systematic errors due to finite model resolution, otherwise identical simulations are run at a range of model resolutions. Notably, to obtain comparable plumes in the different simulations, it is found necessary to use an advection scheme consistent with the Large Eddy Model representation of sub-grid winds for those simulations with degraded resolution. Our simulations show that OH concentration, NO_x lifetime and ozone production efficiency of the model change by 8%, 32% and 31% respectively between the highest (200 m×200 m×40 m) and lowest resolution (9600 m×9600 m×1920 m) simulations. Interpolating to the resolution of a typical global composition transport model (CTM, 5°×5°), suggests that a CTM overestimates OH, NO_x lifetime and ozone production efficiency by approximately 15%, 55% and 59% respectively. For the first time, it is shown explicitly that the reduction in model skill is due to the coarse resolution of these CTMs and the non-linear nature of atmospheric chemistry. These results are significant for the assessment and forecasting of the climate impact of ship NO_x and indicate that for realistic representation of ship plume emissions in CTMs, some suitable parametrisation is necessary at current global model resolutions.

1 Introduction

Oxides of nitrogen (NO_x) play a central role in determining the composition of the atmosphere. A significant source of NO_x is from shipping; however, its inclusion in global atmospheric composition transport models (CTMs) leads to a significant reduction in model skill in simulating the composition of the marine boundary layer (MBL). International shipping consumes 16% of the total fuel for all traffic (road and aviation included) with the ocean-going fleet emitting approximately 9.2 times the NO_x of aviation traffic (Eyring et al., 2005b). Increased industrialization and globalization suggest that ship

ACPD

9, 8587–8618, 2009

emissions will continue to grow at around 3% yr^{-1} (Entec, 2002). By 2050, ship-emitted NO_x could exceed that emitted by present-day road traffic, if the extrapolation is based on an emissions scenario corresponding to high GDP growth (Eyring et al., 2005a). Despite their importance, ship emissions are not typically included in global 3D CTMs as they cause models to significantly overestimate NO_x and O_3 in the MBL (Kasibhatla et al., 2000; Davis et al., 2001; Endersen et al., 2003). This overestimate is usually attributed to the combination of coarse spatial resolution and the non-linear nature of the O_x–HO_x–NO_x chemistry (Song et al., 2003). However, little work has been undertaken to quantify the impact of resolution on ship plumes. In this paper we construct a model specifically to investigate the impact of resolution on the photochemical system and apply it to the emissions from ships. We run the model at various resolutions and then quantify the impact of resolution on the O_x–HO_x–NO_x chemistry of a ship plume.

The high temperature combustion in ship engines leads to emissions high in NO_x, but low in other photo-pollutants such as carbon monoxide (CO) and volatile organic compounds (VOCs) relative to other sources. Corbett and Koehler (2003) found the NO_x emissions from shipping to be 6.87 Tg N yr^{-1} with a 5-th to 95-th percentile spread of 6.19 to 9.15 Tg N yr^{-1}. This can be compared to a global anthropogenic NO_x emission of 33 Tg N yr^{-1} and emissions from all sources of 52 Tg N yr^{-1} (Forster et al., 2007). Whereas most NO_x sources are to be found over land, emissions from shipping occur within the MBL and therefore constitute the only large primary NO_x source in these regions.

Endersen et al. (2003) found significant perturbations to NO_x, NO_y and O_3 within the MBL due to ship emissions and then investigated this impact on the climate system. Their model calculations indicated that the resulting increase in O_3 leads to a radiative forcing since pre-industrial times of 0.029 Wm^{-2}. They also found that the global increase in OH concentrations leads to a decrease in CH_4 concentrations that also has a radiative impact and calculate this to be −0.028 Wm^{-2} since pre-industrial times. These values are around 10% of the total radiative forcing of these gases since pre-industrial times.

Remarkably, tropospheric reactive trace gases ozone (O_3) and methane (CH_4) together contribute approximately as much towards positive global radiative forcing as carbon dioxide (CO_2) (Forster et al., 2007). Emission of oxides of nitrogen (NO_x) plays a crucial role in determining the sources and sinks of O_3 and the lifetime of CH_4 (Logan, 1985). Therefore, understanding the source and chemical fate of NO_x is key to understanding the global chemistry-climate system.

Understanding the processes controlling the composition of the MBL and its photochemistry is of central importance to the chemistry-climate system. Over 50% of CH_4 is destroyed within the MBL (Lawrence et al., 2001) and the MBL constitutes a large sink for O_3. Thus, although far from pollution sources, the MBL plays an important role in removing climatically important trace gases.

Previous studies with global CTMs have found that ship emissions cause large perturbations in the composition of the MBL. Kasibhatla et al. (2000) found the inclusion of ship emissions of NO_x caused a seven-fold increase in the modelled NO_x concentration in the North Atlantic MBL. Lawrence and Crutzen (1999) found that when ship NO_x emissions were included in their global CTM, surface NO_x concentrations increased twofold over much of the northern Atlantic, Pacific and Indian Oceans; O_3 concentrations increased over the central North Atlantic and Pacific Oceans by greater than a factor of 2; and OH increased by more than 20% over similar areas. Even greater model overestimates of NO_x, O_3 and OH were found when the study focused on shipping lanes away from the coasts. In an independent study, Davis et al. (2001) also demonstrated that including ship emissions in a CTM can overestimate the observed median NO_x values by 2.5 to 4 times even when accounting for model bias.

The apparent errors in model chemical budgets associated with ship emissions, including significant overestimate of ozone production, have been attributed by some authors to model resolution effects. In a coarse resolution model, chemical mixing ratios near emissions sites are instantaneously homogenized within the volume of a model grid-box. It is well-established that, due to the nonlinearity of O_x–HO_x–NO_x chemistry, such artificially rapid mixing can lead to systematic changes in net radical

ACPD
9, 8587–8618, 2009

concentrations, and consequently to errors in the tendencies of many radiatively active gases including ozone (Chatfield and Delaney, 1990; Liang and Jacobson, 2000).

The existence of a mechanism leading to the overestimation of ozone production rates in coarse resolution models is apparent if one considers the two distinct chemical regimes that exist near any localised source of NO_x, including ship plumes. At the core of the plume near the source, NO_x concentrations are high, and the ozone production efficiency (OPE), or number of ozone molecules produced per NO_x molecule destroyed, is known to be low (Liu et al., 1987). Further from the source, where the emitted NO_x has been diluted by clean MBL air, the OPE may be many times higher. Generally, clean MBL air has high OPE and a low concentration of NO_x leading to little O_3 production. However, the more rapid the mixing experienced by the plume, the less time a typical NO_x molecule spends in the low OPE regime, and the greater its probability of reaching the high efficiency regime before it is destroyed. If a plume is poorly resolved due to coarse model resolution, the associated artificial mixing will therefore ensure that the average OPE is higher. Esler et al. (2004) have shown the degradation of CTM model fields, from a horizontal resolution of $5.5^\circ \times 5.5^\circ$ (T42) to $2.75^\circ \times 2.75^\circ$ (T21), leads to a systematic increase of 5–10% in OPE throughout the troposphere. In shipping lanes where strong gradients of NO_x exist at the edges of ship plumes, the resolution effect might be expected to be greater, although the details must depend on the details of the emissions and the typical "plume dilution scenario" (Esler, 2003). Establishing whether or not the resolution effect can fully account for the erroneous representation of ship emission effects in CTMs will be one of the main objectives of this study.

However, there may be other explanations for the CTM failure: emissions may be lower than anticipated, heterogeneous chemistry in the plume may remove the NO_x or halogen chemistry within the MBL may lead to enhanced O_3 and NO_x loss rates and enhanced rates of removal. A multi-model study of the global impact of shipping on NO_x and O_3 found that the estimated uncertainty resulting from a combination of the uncertainties in ship emission totals, global distribution of ship emissions and the

neglect of ship plume dispersion was greater than the uncertainties resulting from using the different models (Eyring et al., 2007). Therefore, the ability of resolution to explain the perceived failure of global models to simulate ship NO_x emissions should be tested fully within a model.

This paper is organized as follows. Section 2 describes the physical system we model and in Sect. 3 we give the technical details of our model. In Sect. 4, we discuss the highest resolution runs of our model and then report the results of degrading the model's resolution in Sect. 5. Conclusions are then given in Sect. 6.

2 Physical and chemical scenario

Our goal is to model the emissions plume of a typical merchant ship travelling across the open ocean through the remote MBL. We choose a location based on the Barbados Oceanographic and Meteorological Experiment (BOMEX) project (Holland, 1972) and use wind data derived from an offline run of a large eddy model (LEM) case study of BOMEX (Siebesma and Cuijpers, 1995; Brown, 1999). In this south Atlantic trade wind region (15° N, 54° W), winds are generally light to moderate and there is a shallow layer of non-precipitating cumulus cloud.

The relative mean wind speed in our simulations is taken to be $1\,ms^{-1}$ in the negative x-direction. Typical translation speeds of merchant and military ships used in previous studies range from $7.7–12.6\,ms^{-1}$ (Liu et al., 2000) and $5–12\,ms^{-1}$ (Hobbs et al., 2000), so the prescribed wind field can be interpreted as being relative to the moving ship's frame of reference (i.e. so that the wind speed relative to the ground is in the range $4–11.6\,ms^{-1}$). The current study is therefore focused on the case where the ship is moving in the same direction as a steady breeze. Other ship-relative wind relationships are also of interest (e.g. Song et al., 2003), but due to the difficulty of resolving the plume over a much larger domain, which would require substantially greater computational resources, we choose to concentrate on the aforementioned scenario.

Ship emissions are assumed to take place into initially unpolluted MBL air that is typ-

ACPD
9, 8587–8618, 2009

ical of the subtropical location of the BOMEX experiment. Because most NO_x emitted by fossil fuel combustion consists mainly of NO (EPA, 2000; Hewitt, 2001), our model ship releases NO at a point source, directly into the MBL. The initial trace gas concentrations are assumed to be uniform throughout the MBL and are determined by running the photochemistry model for 25 h with zero emission of NO to establish a diurnal cycle of "clean" MBL chemistry. The clean MBL run was spun-up from concentrations for all species set to zero except for $[O_3]$=30 ppb, $[NO_2]$=30 ppt, $[CH_2O]$, $[CH_3OOH]$ and $[H_2O_2]$ (all 100 ppt). Ship emissions of NO commence at noon local time into the clean MBL background. The variability of NO_x emission scenarios in the literature (Hobbs et al., 2000; Song et al., 2003; Sinha et al., 2003; von Glasgow et al., 2003; Chen et al., 2005) stems from the differences in vessel and engine type and average ship speed under investigation. The range of emission factors spans 12 to 65 g of NO per kg of fuel burned. In our simulation, we emit NO into a single grid-box at the lowest vertical level at a rate of 33 g s^{-1}. This rate is obtained from the case of a medium speed compression ignition marine engine using 50 tons of fuel per day emitting NO_x at a rate of 57 kg per ton of fuel (Corbett and Fischbeck, 1998; Corbett and Koehler, 2003). We have also examined the results of a running lower emission scenario of NO released at a rate of 16 g s^{-1} (not shown).

3 Model equations and numerical implementation

In order to investigate the impact of model resolution on the photochemistry of the MBL we construct a photochemical transport model of the MBL capable of running at a high resolution (compared to a global composition transport model), but also capable of having its numerical grid systematically coarsened to progressively lower resolutions. The model equations to be solved are

$$\frac{\partial q_n}{\partial t} + \boldsymbol{u} \cdot \nabla q_n = H_n(\boldsymbol{q}) + S_n, \; n = 1, \ldots, N, \quad (1)$$

ACPD
9, 8587–8618, 2009

for the vector of chemical species concentrations $\boldsymbol{q}=\{q_1, q_2, \ldots, q_N\}$, where the number of species $N=12$. The initial conditions for all species are set to the uniform MBL concentrations described above in Sect. 2. The source term S_n, which is non-zero only for the species NO, is modelled by instantaneously diluting the total NO emitted over a model time-step into the model grid-cell containing the ship stack. The advecting velocity field $\boldsymbol{u}$ is derived from the output of an LEM simulation, as described in Sect. 3.1. Section 3.2 discusses the advection scheme used to advance the left hand side of Eq. 1. Finally, the details of the chemical species $\boldsymbol{q}$ and chemistry scheme $H_n(\boldsymbol{q})$ are set out in Sect. 3.3.

The model domain is taken to be periodic in the y-direction (cross-flow direction). In the x-direction (along-flow direction), inflow conditions based on clean air MBL concentrations are imposed at the upstream boundary and outflow conditions at the downstream boundary. The dimensions of our high resolution domain are 115.2 km×9.6 km×1.92 km. That region of the LEM domain above 1.92 km (up to 3 km) is modelled by a reservoir of (spatially) uniform concentration air. Free exchange and mixing of air occurs between this reservoir and the main high resolution part of the domain below. Note that the reservoir is located above the level of imposed subsidence (approximately 1.5 km) in the LEM simulation to be described.

The mean wind velocity, relative to the ship stack, in our simulations is taken to be $1\,\mathrm{ms}^{-1}$ in the x-direction. The plume remains in the domain for approximately 36 h before exiting the box at the downstream boundary. Therefore, Eq. (1) is integrated for this period of time in order to model the chemical evolution of the plume until it reaches a near steady state.

3.1 The advecting velocity field: LEM simulation

We use the UK Meteorological Office's Large Eddy Model (version 2.3) (Gray et al., 2001) to provide high resolution winds suitable for the modelling of a ship plume. For the present investigation a classic idealised MBL simulation of trade wind cumulus based on the BOMEX case study (Siebesma and Cuijpers, 1995; Brown, 1999) is cho-

sen. Cumulus-topped boundary layers are common over the worlds oceans; therefore, this is a simulation of an extremely common MBL situation (sensitivities to boundary layer meteorology will be addressed in future work). Additionally, the LEM simulation of BOMEX is appropriate because the model simulations have been extensively evaluated during studies performed within the "Global Energy and Water Cycle Experiment Cloud System Study" (GCSS) programme (Brown, 1999). Consequently, the simulations produce a sufficiently realistic boundary-layer for the purposes of this study.

Version 2.3 of the Met Office large eddy model (LEM) is a non-hydrostatic model that can be run in one, two or three dimensions. The model has periodic lateral boundary conditions, a no-slip base and a free-slip lid. The model setup of Brown (1999) is used, with a larger horizontal domain (9.6 km×9.6 km rather than 6.4 km×6.4 km) and with larger horizontal grid-spacings (200 m rather than 100 m) in order to reduce computational costs. The model domain is 3 km high and the vertical grid-spacing is 40 m. A Newtonian damping layer is applied above 2300 m to prevent the reflection of gravity waves from the top of the model.

Cloud water is modelled with a single moment scheme, and the LEM rain scheme is not switched on. Surface sensible and latent heat fluxes are prescribed (8.04 Wm^{-2} and 130.052 Wm^{-2} respectively) so that in the present experiments there is no diurnal cycle in the model winds. Radiative effects are not explicitly modelled, instead a radiative cooling of 2 K day^{-1} is imposed from the surface to 1500 m, which then decreases linearly to zero at 2500 m. A large-scale subsidence is imposed with a maximum subsidence rate of 0.0065 m s^{-1} at 1500 m (linearly decreasing to zero at the surface and 2100 m). A drying of 1.2×10^{-8} g kg^{-1} s^{-1} is applied from the surface to 300 m (decreasing linearly to zero from 300 to 500 m) to represent large-scale horizontal advective drying in the sub-cloud layer. In addition to the model winds, the LEM simulation also provided temperature and pressure profiles for use in the model chemistry scheme.

Given that the zonal wind speed is approximately 1 m s^{-1} in these simulations, the plume edge will reach the end of the LEM's 9.6 km domain in about 160 min. This is not enough time to simulate the full impact of NO_x emissions on the system. A longer

ACPD
9, 8587–8618, 2009

model domain in the zonal direction is required in order to simulate the 36 h needed to examine the impact of the ship plume on MBL photochemistry. To increase our domain size with the minimum off-line computational expense, we "tile" the output of the LEM along the zonal direction to form an extended domain for the plume to occupy. The periodic boundary condition used for the initial LEM simulation is ideally suited for this. We use 12 tiles, and thus we go from a 9.6 km×9.6 km×1.92 km LEM simulation to a 115.2 km×9.6 km×1.92 km simulation with the chemistry transport model.

The LEM generates wind fields for a 6 h period. The photochemical transport model simulations are run for 36 h so the LEM meteorological fields are reused for each 6 h period of the photochemical transport model integration (see Sect. 3.2 for details). Note that the diurnal cycle in the MBL is not as pronounced as in a boundary layer over land (Stull, 1988); therefore, the absence of a diurnal cycle in the wind fields is not believed to be a major issue for the current study.

3.2 Advection and the degrading of resolution

A standard upwind advection scheme (see e.g. LeVeque, 2002) is used to solve the advection equation for the mean mixing ratio of the active chemical species q_n (n=1, . . .,12), with $\boldsymbol{u}$ derived from the LEM output. Note that the supplied wind-field is non-divergent $\nabla \cdot \boldsymbol{u}=0$. As mentioned above, all simulations are run for 36 h which ensures that transient model behaviour can be eliminated. The LEM winds are supplied at 1 min intervals; we interpolate in time to match our advection time step of 3 sec which is chosen to satisfy the Courant-Friedrichs-Lewy (CFL) condition. Numerical tests established that model solutions are not very sensitive to the degradation in the temporal resolution of the wind fields due to the interpolation in time. After the 6 h of LEM winds have been used, the wind fields are interpolated back to those at t=0 and the time series for $\boldsymbol{u}$ is used again.

A natural first approach to degrade the resolution of the wind fields, for use with a lower resolution version of the advection model, is simply to average the wind component normal to each grid-box boundary. Because the LEM supplies a divergence-free

ACPD
9, 8587–8618, 2009

wind field, the averaging process maintains the divergence-free property of the wind field while rendering it suitable for advection with a coarser grid (i.e. larger grid boxes). Hence, we can calculate a single flux along each edge of the larger grid box. A second alternative to degrade the resolution is to sum the positive and negative wind components normal to each grid-box boundary separately. This approach allows a two-way exchange at each grid box boundary. In Appendix A, we demonstrate with a passive tracer that this second method is considerably more accurate than the first because by using the two-way exchange, we retain the transports due to the unresolved scales of the LEM winds, much as in a sub-grid turbulence closure scheme. If the first (naive) option is used, it is found that the plume spreads too rapidly in the horizontal directions and remains trapped relatively near the surface compared to the higher resolution simulations. The two-way flux scheme therefore allows an important effect of the sub-grid winds to be captured in the lower resolution simulations. In coarse resolution CTMs, a boundary layer turbulence scheme is usually employed to model the same sub-grid wind effects.

The highest resolution gridbox in this study is 200 m×200 m in the horizontal and 40 m in the vertical, which is based on the resolution of the LEM output, and we refer to it as the C1 case. When we coarsen the high resolution domain, we reduce the resolution in all three directions, horizontal and vertical, while maintaining the divergence-free LEM wind field. The result of this coarsening is to increase grid box volumes by n^3 where n=2, 4, 8, 16, 48 and we refer to these cases as Cn in the figures. The two-way flux exchange method we use to coarsen the winds preserves the sub-gridscale winds while coarsening the chemistry model resolution (See Appendix A). This ensures that we maintain a consistent physical form of the plume across model resolutions.

3.3 Chemistry scheme

Our chemistry scheme includes the key interactions of O_x–HO_x–NO_x and the relevant photochemistry in the MBL. We designed the chemical model to focus on the key reactions of NO_x, in the ship plume and surrounding air, with O_3 and the hydroxyl radical

OH. To this end, we follow the evolution of twelve critical species while maintaining other species constant. We hold three species constant over the entire model run: H_2O, CH_4 and CO. These are long-lived species with respect to the model integration time.

Table 1 summarizes the chemical reactions we use to model the tropospheric chemistry in the MBL. The reaction rates are taken from the Master Chemical Mechanism (http://mcm.leeds.ac.uk/MCM/). We model the evolution of twelve chemical species: O_3, NO, NO_2, NO_3, OH, HO_2, CH_3O_2, CH_2O, CH_3OOH, H_2O_2, HNO_3 and N_2O_5. We ignore HNO_2 and HNO_4 chemistry as these species do not play a significant role in the MBL.

The model run begins on Julian day 80, the spring equinox. The solar zenith angle is calculated as a function of date, time of day, latitude and longitude. Vertical profiles of temperature and pressure taken from the LEM model run offline are used to calculate reaction rates for each vertical model level. We use a GEAR (VODE) solver (Brown et al., 1989) to integrate the chemistry component of the system of differential equations (1).

4 Results: high resolution simulations

We allow the model to spin up for 12 h and use only the last 24 h of the simulation in our study. Results are shown for times on the second day of the run and all times are given as local time.

Figure 1 shows the horizontal extent of the NO_x plume at the lowest model level. Highest NO_x concentrations are near the source of NO emission which is the lowest level box located at the eastward edge and at the channel centre in the y-direction (x=115.2 km, y=4.8 km). The NO_x plume is mainly being advected westward relative to the ship stack, and spreads out due to turbulent diffusion downwind of the source. Figure 2 shows a vertical cross-section of the NO_x plume at four locations downstream from the source. The plume height and across-plume width increase with distance

ACPD
9, 8587–8618, 2009

downstream from the source. Note that the plume remains generally trapped in the vertical below the level of imposed subsidence in the LEM model (approximately 1.5 km).

5 Results: impact of resolution

In this section we show how the spatial patterns of NO_x, O_3 and OH concentrations vary as model resolution is changed. We also assess the impact of changing the model resolution by computing the spatial mean over the model domain of several relevant quantities: OH concentrations, NO_x lifetime and O_3 production efficiency. These mean values are calculated at noon (local time) on day 2 of the model integration.

Figure 3 shows snapshots of the lowest vertical level of the ship plume in NO_x, O_3 and OH at noon on day 2 for five different resolutions of horizontal grid box volume: 200 m×200 m×40 m (C1), 400 m×400 m×80 m (C2), 800 m×800 m×160 m (C4), 1600 m×1600 m×320 m (C8) and 3200 m×3200 m×640 m (C16). The plume becomes more diffuse as we coarsen the grid boxes (moving down the page). At all model resolutions we can clearly distinguish the heart of the ship plume as shown in Fig. 3a (left column) by very high NO_x coincident with the O_3 and OH minima in 3b (middle column) and 3c (right column). It is to be expected that when NO_x is at very high levels it will consume O_3 and OH rapidly. At all resolutions, the area within the NO_x plume contour line 3162 ppt overlaps with lower O_3 (<24 ppb) and lower OH concentrations ($<4\times10^6$ molecules cm^{-3}).

For all resolutions, the OH levels are highest in a "halo" which lies on top of the NO_x plume edge where the NO_x values are roughly between 300 and 1000 ppt. This halo is consistent with our knowledge of the OH response to NO_x in tropospheric photochemistry. In their observational work, Sinha et al. (2003) discuss the effect that NO_x and O_3 downwind of ship plumes have on OH, that is, to elevate OH levels, and this enhancement is captured in our simulations at all resolutions.

Figure 4 gives further evidence of this "halo" of enhanced OH in this across-plume 1-D section of OH concentrations at different resolutions. At the edge of the plume,

ACPD
9, 8587–8618, 2009

in the region where the plume air is mixing with the cleaner background air, OH levels are enhanced. This is due to the presence of moderate amounts of NO_x at the plume edge and high levels of O_3 which have not yet been consumed by the NO_x plume. Chen et al. (2005) calculate an average OH value using observed NO_x in ship plumes in conjunction with a photochemical box model and determine that OH in the plume is between 1.2 and 2.7 times higher than in the ambient air. In Fig. 4, we see that OH concentrations at the plume edge are about 1.4 times higher than in the ambient air and can be up to 12 times higher than in the heart of the plume. Depending on where one draws the edge of the plume, mean in-plume OH concentrations can vary a great deal.

Next, we compute a spatial average over the entire 3-D domain (115.2 km×9.6 km×1.92 km) of OH, NO_x lifetime and Ozone Production Efficiency (OPE). OPE is defined as the number of O_3 molecules produced given the number of NO_x molecules consumed in a unit volume and is calculated in the model as the mean ratio of O_x production rate to mean NO_x loss rate (Lin et al., 1988). All three quantities appear to be linearly dependent on resolution for cases C4, C8, C16 and C48 (see Figs. 5, 6 and 7). The two highest resolution cases C1 and C2 appear to asymptote to a similar value in all three figures. In Sec. 3.2, we explained that our coarsening method uses a two-way exchange at the grid box interfaces; we speculate that perhaps for these two highest resolution cases the two-way exchange creates similar enough conditions, for the meteorology used here, that C2 becomes a sufficiently high resolution to achieve the limiting values for our model. Thus, we fit lines to each of the three sets of values, excluding the two highest resolution cases, using a Matlab routine (robustfit.m) which implements robust regression using iteratively re-weighted least-squares (Holland and Welsch, 1977). Using the parameters from the robust linear fit, we then extrapolate our model results to coarser resolutions, comparable to CTM grid boxes of 1°×1°, 4°×4° and 5°×5° (we assume that the CTM grid box height is equivalent to our model height, 1.92 km). We consider these extrapolated values in order to put our work into the context of CTM grid scales and of previous ship emission

ACPD
9, 8587–8618, 2009

studies using box models.

In a study by (von Glasgow et al., 2003), using a global chemistry model where ship emissions were taken to be a constant source at the sea surface, they found that OH can be overestimated by a factor of 2. When the ship plume is explicitly simulated in our model and then the model resolution is coarsened, we find that the mean amount of OH in the domain increases, but by less than a factor of 2. In Fig. 5, we show the mean number of OH molecules for our model run with different grid box volumes and then we extrapolate the results to resolutions compatible with a typical global CTM. The trend is that OH increases by a few percent each time the gridbox area is increased. The slope of the line is about 0.2 which means that for every factor of 10 by which we increase the grid box volume, we can expect an increase of 2×10^5 molecules of OH cm^{-3}.

We define the NO_x lifetime as ratio of concentration of NO_x to rate of loss of NO_x, where, in our model, the NO_x loss rate is equivalent to the production rate of nitric acid (HNO_3). First, we calculate the domain mean quantities, mass-weighted in the vertical, of NO_x loss and HNO_3 production rate and then compute the ratio. In our results, the spatial variability of NO_x lifetime is extremely high across the domain when a ship plume is present. But if we look at the domain mean, NO_x lifetime decreases steadily with coarsening model resolution. Figure 6 shows that by decreasing spatial resolution we decrease the mean lifetime of NO_x, but only by fractions of an hour. In fact, according to our linear fit, if we increase the grid box volume by a factor of 10, we can expect a decrease of 0.34 h or 20 min. The negative trend in NO_x lifetime is anti-correlated with OH levels and as suggested by (Chen et al., 2005) could indicate that the reaction of OH with NO_2 to produce HNO_3 is the main process by which NO_x is lost. In fact, in our model, the NO_x loss rate is defined as the production rate of HNO_3.

Song et al. (2003) speculated that NO_x lifetime would be 2.5–10 times shorter in the ship plume than in the MBL environment. Chen et al. (2005) measured NO_x in two ship plumes 100 km off the California coast, which they state may have been diluting rapidly due to the ship's heading and meteorological conditions and therefore, may have had

ACPD
9, 8587–8618, 2009

below-average emission concentrations. Then, using a model of exponential decay with plume age and the observations as input Chen et al. (2005) calculated in-plume NO_x lifetime to be approximately 113±23 min. In their study, at noon in the "moderately polluted" background air, NO_x lifetime was about 6.5 h, about 4.7 h longer than in the ship plume. We calculated the mean NO_x lifetime in the entire domain (not shown) for a model run with a ship plume and without at different resolutions and found that the presence of a ship emitting NO decreases the mean NO_x lifetime in the domain by approximately 2 h, less than half the difference found in their study. The difference may be due to the fact that in our model the plume is not experiencing rapid dilution in contrast to the observed ship plumes used as input to their model which were possibly very dilute.

Davis et al. (2001) suggest that global CTMs overestimate NO_x because high concentrations of OH in-plume reduce NO_x lifetime in-plume. We find that OH concentrations are highest (Figs. 3c and 4) and induce the shorter lifetime of NO_x not in the plume core but on the edge of the plume in the aforementioned OH "halo" region. Such spatial detail is impossible to represent if ship plumes not resolved in a model.

Figure 7 shows the OPE at noon on day 2 averaged over all grid boxes in all resolution cases. OPE increases sharply as the grid is coarsened; the slope is about 0.58 which translates to an increase in OPE of 0.58 if the grid box volume increases by a factor of 10. OPE of the run on the coarsest grid (C48) is 31% more than the C1 case. If we extrapolate for larger grid box volumes as we did for mean OH and NO_x lifetime, we can see that a $5^\circ \times 5^\circ$ grid box model would have a mean OPE larger than 10, a clear overestimate of the high resolution ship plume simulation of about 59%.

As we degrade model resolution we find that the same ship emission rate affects the photochemistry of the MBL in significant ways. In the ship emission runs, when the model resolution decreases from C1 to C48: OH increases by 8%, NO_x lifetime decreases by about 32% and OPE increases by 31%. If we forecast using the linear fit, consider that the highest resolution case has 15% less OH than the $5^\circ \times 5^\circ$ case, 55% longer NO_x lifetime and 59% less OPE. When the ship emission rate is halved to

ACPD
9, 8587–8618, 2009

$16\,g\,s^{-1}$ (not shown), OH increases with increasing grid box volume but is less steep. The trend for NO_x lifetime is still negative, but less steep and hence remains anti-correlated with the trend in OH. In the case of OPE, the lower emission rate generates a stronger increase in OPE with coarsening resolution so that a factor of 10 increase in grid box volume results in 0.82 increase in OPE.

When we run the model with a completely clean environment (i.e. no ship emissions) for 36 h, the domain mean values on day 2 at noon for OH, NO_x lifetime and OPE are 5.8×10^6 molecules cm^{-3}, 6.4 h, and 21.3, respectively. Comparing the model clean run, without ship emissions to that with ship emissions, OH increases 59%–72% (C1–C48) in the presence of ship emissions, NO_x lifetime decreases 21%–46% (C1–C48) and OPE decreases 61%–70% (C1–C48).

6 Conclusions

We have built a high spatial resolution model of the chemistry of the MBL with the inclusion of a point source of NO representing emissions from a ship. A range of identical simulations are run in which we vary the spatial resolution to investigate the effect of resolution on the OH concentration, lifetime of NO_x and OPE. We find that the impacts of the ship NO emissions on the MBL chemistry are highly dependent on the model resolution. Within the range of resolutions investigated, OH concentrations increase by about 8% between the highest and lowest resolution simulations. Interpolating this to a resolution typical of CTMs would imply approximately a 15% overestimation of the impact of ship NO_x on MBL OH concentrations calculated by these models. NO_x lifetime is anti-correlated with OH levels which is in agreement with the results of Chen et al. (2005) and could be seen as evidence that the reaction of OH with NO_2 is the key to loss of NO_x. The ozone production efficiency increases by 31% between the highest and lowest resolution simulated here. Interpolating to the scales typical of CTMs we suggest an overestimation of the ozone production by ship emissions within CTMs of approximately 59%. We conclude that spatial resolution has a significant impact on the

ACPD
9, 8587–8618, 2009

simulation of the chemistry of ship emissions in the MBL.

An interesting issue is the turning over or leveling off of the mean values in Figs. 5, 6 and 7. To explore the significance of the shape of this curve, one could run the LEM at a higher horizontal resolution, $50 \times 50\,m^2$ and use the resulting winds to advect the chemical species. This would provide evidence as to whether or not the mean values of OH, NO_x lifetime and OPE are approaching a limiting value.

In the future this modelling framework will be used to focus on the impact of different meteorological scenarios, different emission fluxes and ship velocities with the aim of producing a parametrisation for inclusion in CTMs. Specifically, it would be interesting to run the model with a convectively active, overturning wind circulation. One would expect such a circulation to cause dramatically different plume dynamics, changing the spatial pattern of dilution and perhaps affecting the "halo" of OH as well.

The results presented here are a starting point from which to map out the level or degree of uncertainty due to the neglect of ship plume dispersion and chemistry that currently plague CTM studies of the impact of NO_x emission on O_3 production. They may also have significant implications for other plumes such as from power stations. Finally, our results suggest that better parametrisations of ship emissions in global models need to be designed using, for example, the "equivalent emissions" concept introduced in Esler (2003).

Appendix A

To solve the advection equation

$$\frac{\partial q_n}{\partial t} + \boldsymbol{u} \cdot \nabla q_n = H_n(\boldsymbol{q}) + S_n, \tag{A1}$$

where the wind field is divergence-free ($\nabla \cdot \boldsymbol{u} = 0$) and where q_n is the average concentration of the n-th chemical species, we calculate the flux between grid boxes using the

ACPD
9, 8587–8618, 2009

velocities at the box edges (in the x, y and z directions in turn). For example, one can define the vertical flux at the bottom of box (i, j, k) $F_{i,j,k-1/2}$ as

$$F_{i,j,k-1/2} = w_{i,j,k-1/2} \frac{\delta A \delta t}{\delta V} \quad \text{(A2)}$$

where $w_{i,j,k-1/2}$ is the velocity at the bottom edge of the box, δA is the area of the base of the grid box, δt is the advection time step and δV is the volume of the grid box. Let $q_{ijk}^{(t)}$ be the mean concentration of a particular species in gridbox (i, j, k) at time t. If, for example, $F_{i,j,k+1/2}>0$ and $F_{i,j,k-1/2}>0$ then we update the mean concentration in the vertical direction in the following way:

$$q_{ijk}^{(t+\delta t)} = (1 - F_{k+1/2}) q_{ijk}^{(t)} + F_{k-1/2} q_{i,j,k-1}^{(t)}. \quad \text{(A3)}$$

We coarsen the model resolution by increasing grid box volume. To advect the chemical species between the larger grid boxes we can simply average the winds along each grid box edge and calculate the fluxes with the resulting mean winds. If we choose this method, then each time we coarsen the model resolution we average more of the LEM wind components together thereby losing spatial variability in the wind. By averaging the wind field we stand to lose scales of motion that were originally resolved by the LEM simulation.

Another method retains all of the high resolution winds and calculates a net flux into each box edge and out of each box edge at each level of coarser resolution. For this two-way flux scheme, we must calculate the total negative F^- and positive F^+ fluxes at each grid box edge:

$$F^-_{i,j,k-1/2} = \sum_{i,j:w_{i,j,k-1/2}<0} w_{i,j,k-1/2} \frac{\delta a \delta t}{\delta V} \quad \text{(A4)}$$

$$F^+_{i,j,k-1/2} = \sum_{i,j:w_{i,j,k-1/2}>0} w_{i,j,k-1/2} \frac{\delta a \delta t}{\delta V} \quad \text{(A5)}$$

ACPD
9, 8587–8618, 2009

where δa is the area of the highest resolution grid box side and not the area of the larger volume box at a coarser grid resolution. Now the update for the mean concentration in box (i, j, k) is

$$q_{ijk}^{(t+\delta t)} = (1 - F^{-}_{i,j,k-1/2} - F^{+}_{i,j,k+1/2}) q_{ijk}^{(t)} + F^{+}_{i,j,k-1/2} q^{(t)}_{i,j,k-1} + F^{-}_{i,j,k+1/2} q^{(t)}_{i,j,k+1} \quad \text{(A6)}$$

regardless of the sign of the wind component.

Using the example of a passive tracer, Fig. 8 demonstrates how the two-way flux scheme is superior to the wind averaging scheme as a method of coarsening the model resolution. Figure 8, panels a and c show a vertically averaged plume and panels b and d show a horizontally (along-plume) averaged plume including the emission site. The black dot shows the location of the passive tracer source. The solid lines in all panels are the result of advecting at the highest resolution, but averaging the concentration over a coarse grid box volume. The top two panels (a, b) compare the high resolution advection (thin lines) to the coarsening method by averaging wind fields and performing a single flux exchange at the grid box boundary (thick lines), using the wind averaging technique. The bottom panels (c, d) compare the high resolution advection (thin lines) to the two-way exchange at the boundaries (thick lines). It is evident that the two-way exchange matches the highest resolution plume in vertical and horizontal extent much better than the wind averaging scheme. The wind averaging scheme causes the tracer to flatten out in the horizontal and dimishes its vertical extent. Therefore, we use the two-way exchange method to model all the degraded resolutions cases of the ship plume.

References

Brown, A. R.: The sensitivity of large-eddy simulations of shallow cumulus convection to resolution and subgrid model, Q. J. Roy. Meteor. Soc., 125, 469–482, 1999. 8592, 8594, 8595

Brown, P. N., Byrne, G. D., and Hindmarsh, A. C.: VODE: A variable coefficient ODE solver, SIAM J. Sci. Stat. Comp., 10, 1038–1051, 1989. 8598

Chatfield, R. B. and Delaney, A. C.: Convection links biomass burn- ing to increased tropical ozone: However, Models will tend to overpredict O_3, J. Geophys. Res., 95, 18 473–18 488, 1990. 8591

Chen, G., Huey, L. G., Trainer, M., Nicks, D., Corbett, J., Ryerson, T., Parrish, D., Neuman, J. A., Nowak, J., Tanner, D., Holloway, J., Brock, C., Crawford, J., Olson, J. R., Sullivan, A., Weber, R., Schauffler, S., Donnelly, S., Atlas, E., Roberts, J., Flocke, F., Hubler, G., and Fehsenfeld, F.: An investigation of the chemistry of ship emission plumes during ITCT 2002, J. Geophys. Res., 110, D10S90, doi:10.1029/2004JD005236, 2005. 8593, 8600, 8601, 8602, 8603

Corbett, J. J. and Fischbeck, P.: Commercial Marine Emissions Inventory for EPA Category 2 and 3 Compression ignition marine engines in United States continental and inland waterways, Tech. rep., US Environmental Protection Agency, 58 pp., 1998. 8593

Corbett, J. J. and Koehler, H. W.: Updated emissions from ocean shipping, J. Geophys. Res., 108(D20), 4650, doi:10.1029/2003JD003751, 2003. 8589, 8593

Davis, D. D., Grodzinsky, G., Kasibhatla, P., Crawford, J., Chen, G., Liu, S., Bandy, A., Thornton, D., Guan, H., and Sandholm, S.: Impact of ship emissions on marine boundary layer NO_x and SO_2 distributions over the Pacific basin, Geophys. Res. Lett., 28, 235–238, 2001. 8589, 8590, 8602

Endersen, O., Sorgard, E., Sundet, J. K., Dalsoren, S. B., Isaksen, I. S. A., Berglen, T. F., and Gravir, G.: Emission from international sea transportation and environmental impact, J. Geophys. Res., 108, 5460, 2003. 8589

Entec UK Ltd.: Quantification of emissions from ships associated with ship movements between ports in the European Community, Tech. rep., European Commission, 48 pp., 2002. 8589

EPA: Analysis of commercial marine vessels emissions and fuel consumption data, Tech. Rep. EPA420-R-00-002, United States Environmental Protection Agency, 158 pp., 2000. 8593

Esler, J. G.: An integrated approach to mixing sensitivities in tropospheric chemistry: A basis for the parameterization of subgrid-scale emissions for chemistry transport models, J. Geophys. Res., 108(D20), 4632, doi:10.1029/2003JD003627, 2003. 8591, 8604

Esler, J. G., Roelofs, G. J., Köhler, M. O., and O'Connor, F. M.: A quantitative analysis of grid-related systematic errors in oxidising capacity and ozone production rates in chemistry transport models, Atmos. Chem. Phys., 4, 1781–1795, 2004, http://www.atmos-chem-phys.net/4/1781/2004/. 8591

Eyring, V., Kohler, H. W., Lauer, A., and Lemper, B.: Emissions from international shipping: 2. Impact of future technologies on scenarios until 2050, J. Geophys. Res., 110, D17306,

doi:10.1029/2004JD005620, 2005a. 8589
Eyring, V., Kohler, H. W., van Aardenne, J., and Lauer, A.: Emissions from international shipping: 1. The last 50 years, J. Geophys. Res., 110, D17305, doi:10.1029/2004JD005619, 2005b. 8588
Eyring, V., Stevenson, D. S., Lauer, A., Dentener, F. J., Butler, T., Collins, W. J., Ellingsen, K., Gauss, M., Hauglustaine, D. A., Isaksen, I. S. A., Lawrence, M. G., Richter, A., Rodriguez, J. M., Sanderson, M., Strahan, S. E., Sudo, K., Szopa, S., van Noije, T. P. C., and Wild, O.: Multi-model simulations of the impact of international shipping on Atmospheric Chemistry and Climate in 2000 and 2030, Atmos. Chem. Phys., 7, 757–780, 2007, http://www.atmos-chem-phys.net/7/757/2007/. 8592
Forster, P., Ramaswamy, V., Artaxo, P., Berntsen, T., Betts, R., Fahey, D. W., Haywood, J., Lean, J., Lowe, D. C., Myhre, G., Nganga, J., Prinn, R., Raga, G., Schulz, M., and Van Doland, R.: Climate Change 2007: The Physical Science Basis, Cambridge University Press, 996 pp., 2007. 8589, 8590
Gray, M. E. B., Petch, J., Derbyshire, S. H., Brown, A. R., Lock, A. P., and Swann, H. A.: Version 2.3 of the Met. Office large eddy model, Tech. rep., The Met. Office, Exeter, UK, 2001. 8594
Hewitt, C. N.: The atmospheric chemistry of sulphur and nitrogen in power station plumes, Atmos. Environ., 35, 1155–1170, 2001. 8593
Hobbs, P. V., Garrett, T. J., Ferek, R. J., Strader, S. R., Hegg, D. A., Frick, G. M., Hoppel, W. A., Gasparovic, R. F., Russell, L. M., Johnson, D. W., O'Dowd, C., Durkee, P. A., Nielsen, K. E., and Innis, G.: Emissions from Ships with respect to Their Effects on Clouds, J. Atmos. Sci., 57, 2570–2590, 2000. 8592, 8593
Holland, J. Z.: Comparative evaluation of some BOMEX measurements of sea surface evaporation, energy flux and stress, J. Phys. Oceanogr., 2, 476–486, 1972. 8592
Holland, P. W. and Welsch, R. E.: Robust regression using iteratively reweighted least-squares, Communications in Statistics: Theory and Methods, A6, 813–827, 1977. 8600
Kasibhatla, P., Levy II, H., Moxim, W. J., Pandis, S. N., Corbett, J. J., Peterson, M. C., Honrath, R. E., Frost, G. J., Knapp, K., Parrish, D. D., and Ryerson, T. B.: Do emissions from ships have a significant impact on the concentrations of nitrogen oxides in the marine boundary layer?, J. Geophys. Res., 27, 2229–2232, 2000. 8589, 8590
Lawrence, M. G. and Crutzen, P. J.: Influence of NOx emissions from ships on tropospheric photochemistry and climate, Nature, 402, 167–170, 1999. 8590

Lawrence, M. G., Jöckel, P., and von Kuhlmann, R.: What does the global mean OH concentration tell us?, Atmos. Chem. Phys., 1, 37–49, 2001, http://www.atmos-chem-phys.net/1/37/2001/. 8590

LeVeque, R. J.: Finite Volume Methods for Hyperbolic Problems, Cambridge University Press, 578 pp., 2002. 8596

Liang, J. and Jacobson, M. Z.: Effects of subgrid segregation on ozone production efficiency in a chemical model, Atmos. Environ., 34, 2975–2982, 2000. 8591

Lin, X., Trainer, M., and Liu, S. C.: On the nonlinearity of the tropospheric ozone production, J. Geophys. Res., 93(D12), 15 879–15 888, 1988. 8600

Liu, Q., Kogan, Y., Lilly, D. K., Johnson, D., Innis, G. E., Durkee, P. A., and Nielsen, K. E.: Modeling of Ship Effluent Transport and Its Sensitivity to Boundary Layer Structure, J. Atmos. Sci., 57, 2779–2791, 2000. 8592

Liu, S. C., Trainer, M., Fehsenfeld, F. C., Parrish, D. D., Williams, E. J., Fahey, D. W., Hübler, G., and Murphy, P. C.: Ozone production in the rural troposphere and the implications for regional and global ozone distributions, J. Geophys. Res., 92(D4), 4191–4207, 1987. 8591

Logan, J. A.: Tropospheric Ozone: seasonal behavior, trends and anthropogenic influence, J. Geophys. Res., 90, 10 463–10 482, 1985. 8590

Siebesma, A. P. and Cuijpers, J. W. M.: Evaluation of Parametric Assumptions for Shallow Cumulus Convection, J. Atmos. Sci., 52, 650–666, 1995. 8592, 8594

Sinha, P., Hobbs, P. V., Yokelson, R. J., Christian, T. J., Kirchstetter, T. W., and Bruintjes, R.: Emissions of trace gases and particles from two ships in the southern Atlantic Ocean, Atmos. Environ., 37, 2139–2148, 2003. 8593, 8599

Song, C. H., Chen, G., Hanna, S. R., Crawford, J., and Davis, D. D.: Dispersion and chemical evolution of ship plumes in the marine boundary layer: Investigation of $O_3/NO_y/HO_x$ chemistry, J. Geophys. Res., 108(D4), 4143, doi:10.1029/2002JD002216, 2003. 8589, 8592, 8593, 8601

Stull, R.: An Introduction to Boundary Layer Meteorology, Kluwer Academic Publishers, 666 pp., 1988. 8596

von Glasow, R., Lawrence, M. G., Sander, R., and Crutzen, P. J.: Modeling the chemical effects of ship exhaust in the cloud-free marine boundary layer, Atmos. Chem. Phys., 3, 233–250, 2003, http://www.atmos-chem-phys.net/3/233/2003/. 8593, 8601

Table 1. Chemical reactions modelled. Derived from the Master Chemical Mechanism where ζ is solar zenith angle; T temperature [K]; p pressure [hPa]; and m number density of air [molecules cm^{-3}]. k_{12} reaction product is H_2O; k_{18} represents PAN decomposition; k_{19} represents the heterogeneous uptake of N_2O_5.

$O_3+h\nu \rightarrow O^1D$	$J_1=6.073\times10^{-5}\cos(\zeta^{1.743})\exp(-0.474/\cos\zeta)$
$NO_2+h\nu \rightarrow NO+O_3$	$J_2=1.165\times10^{-2}\cos(\zeta^{0.244})\exp(-0.267/\cos\zeta)$
$CH_2O+h\nu \rightarrow CO$	$J_3=6.853\times10^{-5}\cos(\zeta^{0.477})\exp(-0.353/\cos\zeta)$
$CH_2O+h\nu \rightarrow CO+2HO_2$	$J_4=4.642\times10^{-5}\cos(\zeta^{0.762})\exp(-0.353/\cos\zeta)$
$NO_3+h\nu \rightarrow NO$	$J_5=2.485\times10^{-2}\cos(\zeta^{0.168})\exp(-0.108/\cos\zeta)$
$NO_3+h\nu \rightarrow NO_2+O_3$	$J_6=1.747\times10^{-1}\cos(\zeta^{0.155})\exp(-0.125/\cos\zeta)$
$NO+O_3 \rightarrow NO_2$	$k_3=1.4\times10^{-12}\exp(-1310/T)$
$OH+CO \rightarrow HO_2$	$k_4=1.30\times10^{-13}$
$OH+CH_4 \rightarrow CH_3O_2$	$k_5=9.65\times10^{-20}\ (T^{2.58})\exp(-1082/T)$
$HO_2+NO \rightarrow OH+NO_2$	$k_6=3.6\times10^{-12}\exp\ (270/T)$
$HO_2+O_3 \rightarrow OH$	$k_7=2.03\times10^{-16}\ (T/300)^{4.57}\exp(693/T)$
$CH_3O_2+NO \rightarrow NO_2+CH_2O+HO_2$	$k_8=1.82\times10^{-13}\exp\ (416/T)$
$CH_3O_2+HO_2 \rightarrow CH_3OOH+O_2$	$k_9=3.80\times10^{-13}\exp\ (780/T)$
$HO_2+HO_2 \rightarrow H_2O_2$	$k_{10}=2.20\times10^{-13}\exp(600/T)+m1.90\times10^{-33}\exp(980/T)$
$OH+NO_2 \rightarrow HNO_3$	$k_{11}=k_0k_if/(k_0+k_i)\quad[k_0=m\ 3.3\times10^{-30}(T/300)^{-3}, k_i=4.1\times10^{-11},$ $f=10^{\{\log_{10}0.4/(1+(\log_{10}(k_0/k_i))^2)\}}]$
$OH+HO_2 \rightarrow$	$k_{12}=4.80\times10^{-11}\exp(250/T)$
$CH_3O_2+CH_3O_2 \rightarrow$	$k_{13}=1.82\times10^{-13}\exp(416/T)$
$NO_2+O_3 \rightarrow NO_3$	$k_{14}=1.40\times10^{-13}\exp(-2470/T)$
$NO+NO_3 \rightarrow 2NO_2$	$k_{15}=1.80\times10^{-11}\exp(110/T)$
$NO_2+NO_3 \rightarrow N_2O_5$	$k_{16}=k_0k_if/(k_0+k_i),\ [k_i=1.90\times10^{-12}(T/300)^{0.2}$ $k_0=m\,3.60\times10^{-30}(T/300)^{-4.1}, f=10^{\{\log_{10}0.35/(1+(\log_{10}(k_0/k_i))^2)\}}]$
$N_2O_5 \rightarrow NO_2+NO_3$	$k_{17}=k_0k_if/(k_0+k_i),\ [f=10^{\{\log_{10}0.35/(1+(\log_{10}(k_o/k_i))^2)\}}$ $k_0=m\,1.00\times10^{-3}(T/300)^{-3.5}\exp(-11\,000/T)$ $k_i=9.7\times10^{14}(T/300)^{0.1}\exp(-11\,080/T)]$
$\rightarrow NO_2$	$k_{18}=9.25\times10^{3}$
$N_2O_5 \rightarrow 2HNO_3$	$k_{19}=4.0\times10^{-4}$
$NO_2+NO_3 \rightarrow NO_2+NO$	$k_{20}=4.50\times10^{-14}\exp(-1260/T)$

ACPD
9, 8587–8618, 2009

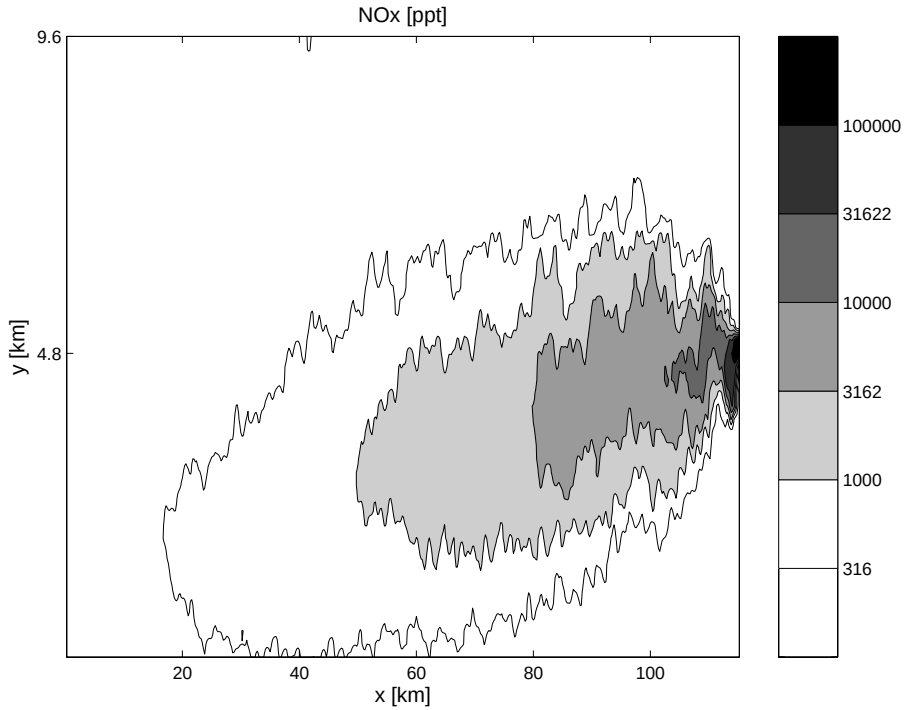

Fig. 1. Lowest vertical level of the NO_x ($NO+NO_2$) plume in the highest resolution (C1) experiment at noon (local time) on day 2, after the plume has evolved for 24 h. Darker shading indicates higher NO_x concentrations. Contour intervals are base 10 logarithmic in units of ppt.

ACPD
9, 8587–8618, 2009

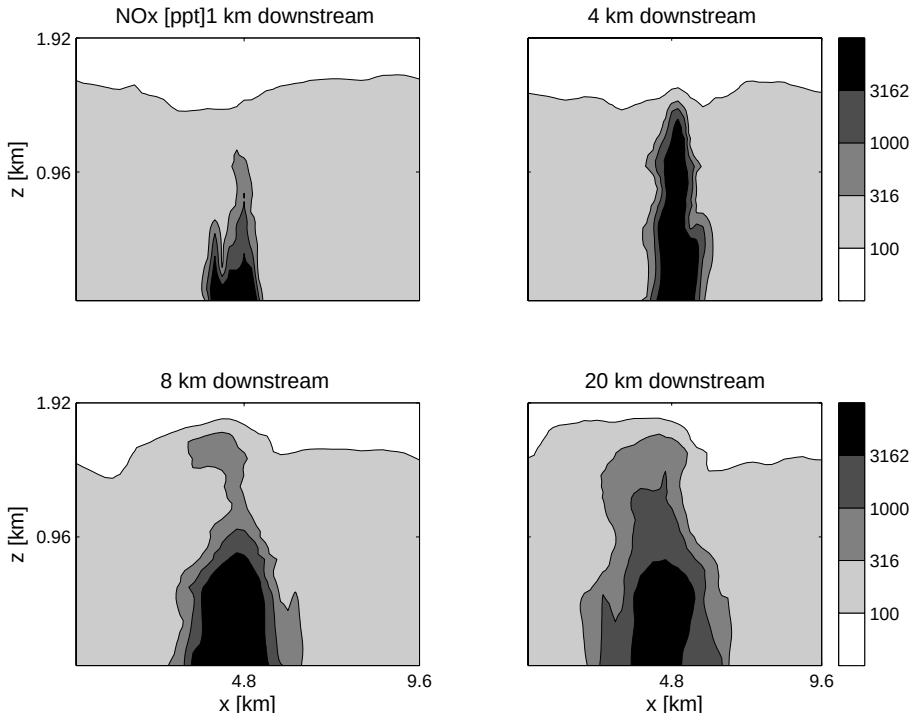

Fig. 2. Vertical sections of NO_x across the plume at noon (local time) on day 2 for the highest resolution (C1) experiment at 1, 4, 8 and 20 km downstream from the source. Contour intervals are base 10 logarithmic in units of ppt.

ACPD
9, 8587–8618, 2009

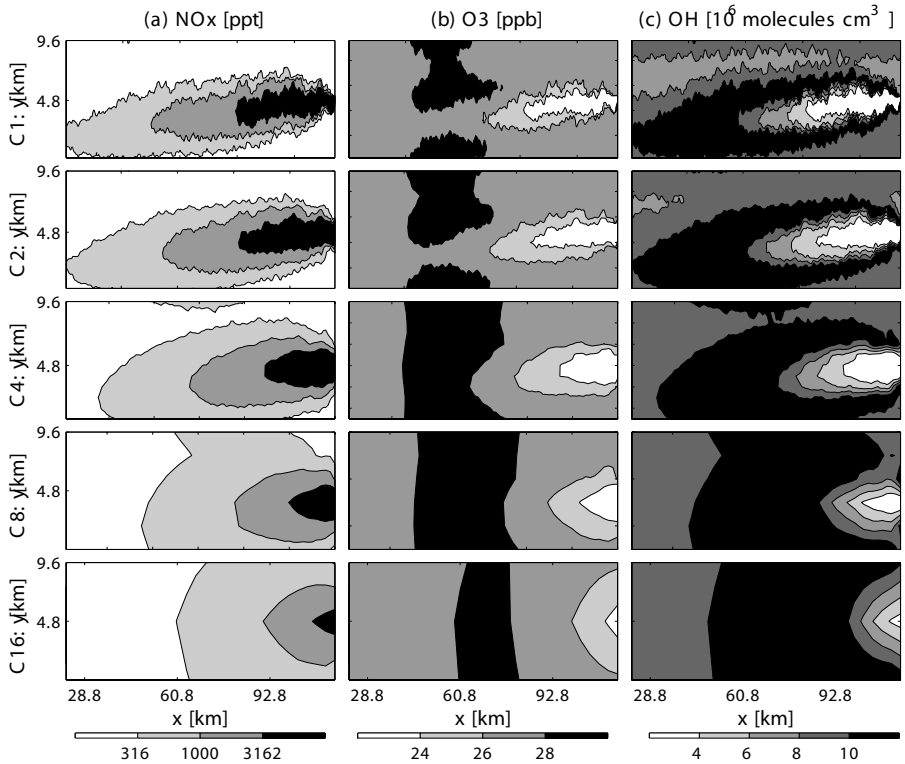

Fig. 3. Lowest vertical level of plume in NO_x **(a)**, O_3 **(b)** and OH **(c)** at noon (local time) on day 2 for five different model resolutions. First row shows the highest resolution C1, then below C2, C4, C8 and C16.

ACPD
9, 8587–8618, 2009

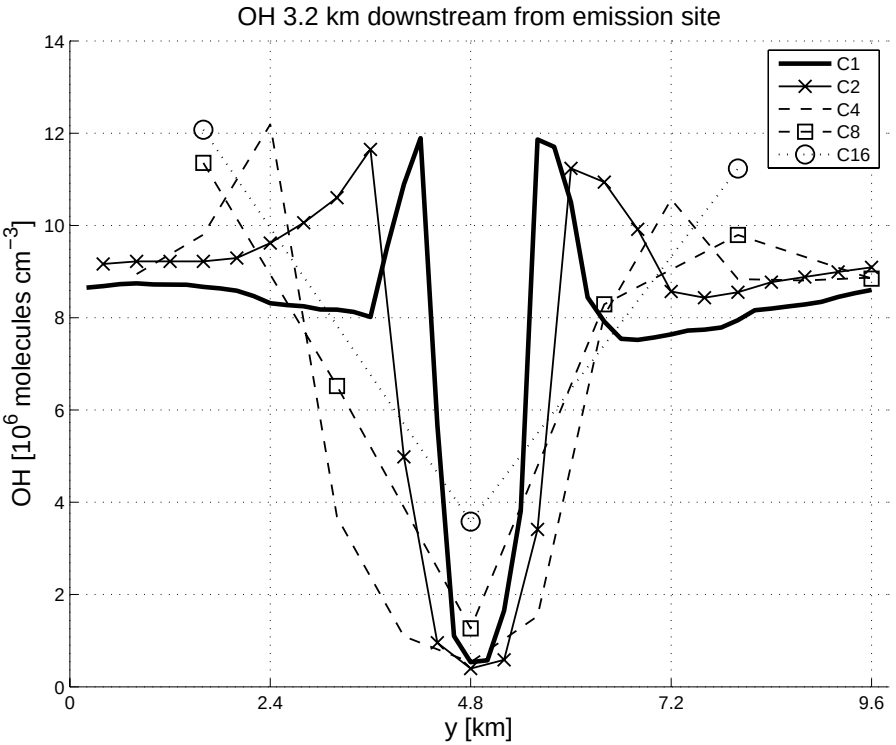

Fig. 4. OH concentrations across the plume on the lowest vertical level 3.2 km downstream of the emission source for four different resolution runs at noon (local time) on day 2.

ACPD
9, 8587–8618, 2009

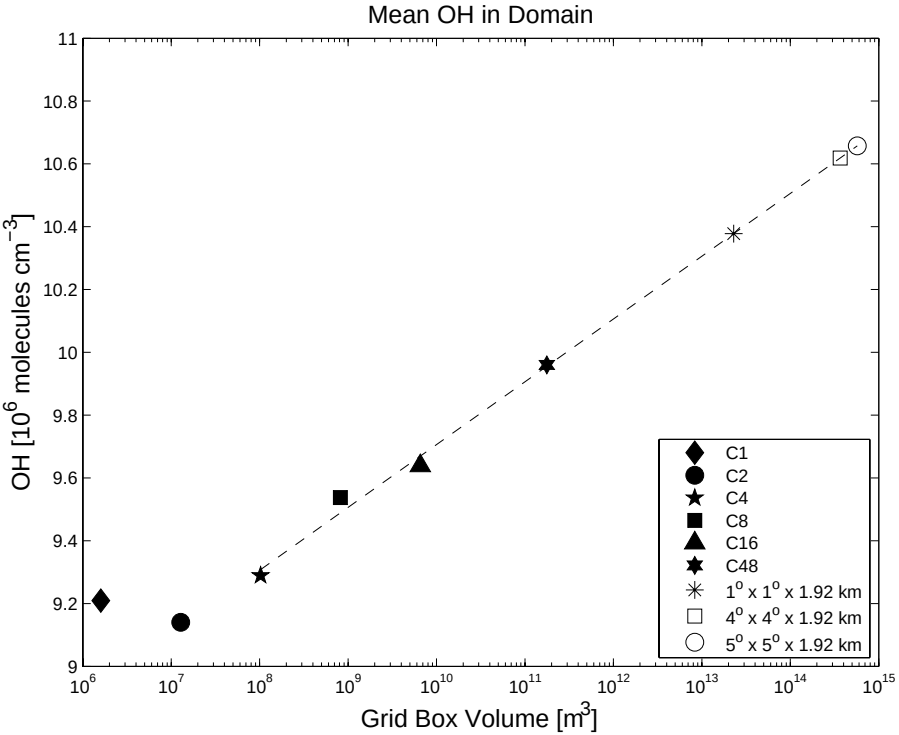

Fig. 5. Domain mean OH at noon (local time) on day 2 for different resolutions. Dashed line represents best fit to the model results C4, C8, C16 and C48. Solid markers represent our model results and hollow ones are the result of linear extrapolation of our results to larger grid box volume sizes. These larger grid box volumes represent typical CTM resolution with a boundary layer height assumed to be that of our model (1.92 km). For comparison, a "no emissions" model run produces a domain mean OH of 5.8×10^6 molecules cm^{-3} at the same time.

ACPD
9, 8587–8618, 2009

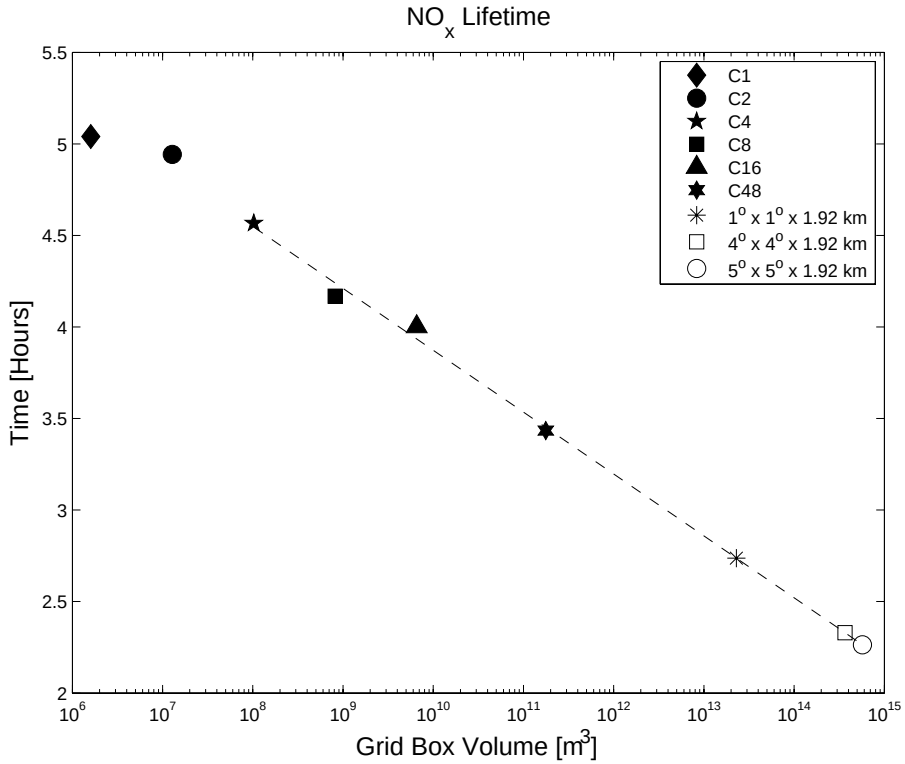

Fig. 6. Mean NO_x lifetime, (defined as the ratio of domain total rate of production of HNO_3 to domain total NO_x), at noon (local time) on day 2 for different resolution domains. Dashed line represents best fit to the model results C4, C8, C16 and C48. Extrapolation as in Fig. 5. For comparison, the clean model run produces a domain mean NO_x lifetime of 6.4 h at the same time.

ACPD
9, 8587–8618, 2009

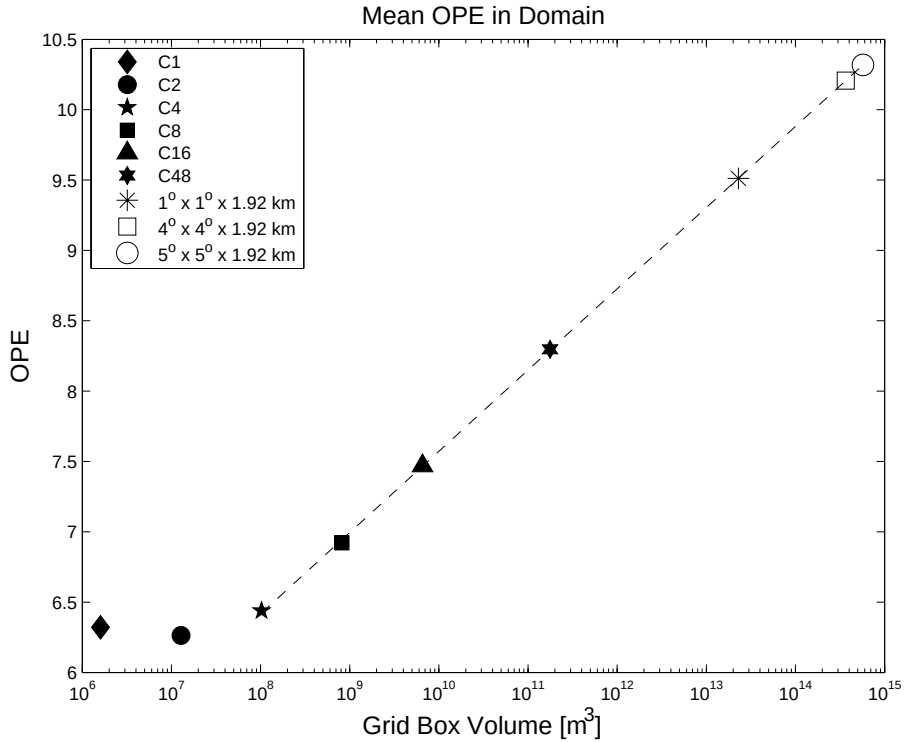

Fig. 7. Domain mean OPE at 12:30 (local time) on day 2 for different resolutions. Dashed line represents best fit to the model results C4, C8, C16 and C48. Extrapolation as in Fig. 5. For comparison, the clean model run produces a domain mean OPE of 21.3 at the same time.

ACPD
9, 8587–8618, 2009

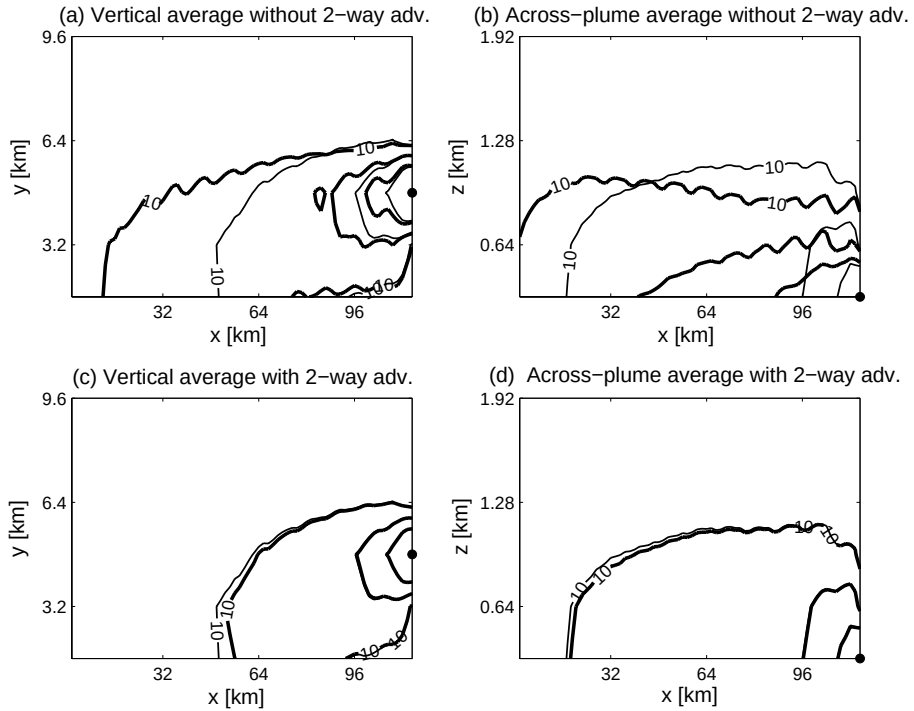

Fig. 8. Passive tracer concentration averaged over vertical **(a, c)** and averaged across the plume **(b, d)** after 18 h. Thin lines in all panels show the model with advection at highest resolution and averaging of chemical concentrations over gridboxes equivalent to the C8 coarsening case. The thick lines represent the concentrations of the coarsened advection (C8) with two-way exchange turned on **(c, d)** and advection without the two-way exchange **(a, b)**. Contour intervals are 10 ppb and contour lines decrease away from the source (black dot).

ACPD
9, 8587–8618, 2009

CC BY